International Journal of Biology and Life Sciences
ISSN: 2957-9511 | Vol. 6, No. 2, 2024

Investigation into the Mechanism of ATP-Induced Senescence Treated with Hegu and Taichong Electroacupuncture

Wei Wang [1], Jinxia Bai [1], Yuting Yang [1], Yanfei Wang [1], Hongfan Li [2], Doblin Sandai [3], Haoling Zhang [3], Zhijing Song [2, *]

[1] College of Acupuncture-Moxibustion and Tuina, Gansu University of Chinese Medicine, Lanzhou, Gansu, China
[2] Clinical College of Chinese Medicine, Gansu University of Chinese Medicine, Lanzhou, Gansu, China
[3] Department of Biomedical Sciences, Advanced Medical and Dental Institute, University Sains Malaysia, Kepala Batas, Penang, Malaysia
*** Corresponding author:** Zhijing Song (Email: Songzhijing2020@163.com)

Abstract: Objective: The purpose of this study was to clarify the aging mechanism of ATP injection combined with Electroacupuncture at Hegu and Taizhong points, and to provide scientific basis for subsequent clinical research. Methods: 60 rats were randomly divided into 5 groups: control group was injected with normal saline; Model group rats were injected with ATP solution; In the intervention group, the frequency of electroacupuncture was 20Hz, 30Hz and 50Hz, respectively. Electroacupuncture at Hegu Point and Taizhong point once a day for 20 minutes each time. Blood RNA was extracted by TRIzol method, and gene sequencing was performed to identify the differential genes. In addition, the "Senescence" gene data was retrieved from the NCBI gene database and intersected with the sequencing data. The core genes were analyzed by enrichment analysis, module analysis, miRNA-mRNA regulatory network analysis and PCR validation. In addition, cell cycle, apoptosis, ROS levels, and mitochondrial membrane potential were evaluated. Results: DGE analysis found 3,510 DEGs in the sequencing data, of which 3,487 up-regulated genes and 23 down-regulated genes. According to KEGG, These genes are mainly involved in the T cell receptor signaling pathway, Human T−cell leukemia virus 1 infection, Protein processing in endoplasmic reticulum and Phosphatidylinositol signaling system. The 59 common genes of aging identified by Venn diagram analysis, KEGG was mainly involved in AGE−RAGE signaling pathway in diabetic complications, Non−alcoholic fatty liver disease and FoxO signaling pathway and other pathways. Venn diagram is used to show the seven core genes identified by all four algorithms: HSPA4, CASP3, AKT1, PARP1, NFKB1, GSK3B, FOXO3. Electroacupuncture can inhibit apoptosis in ATP-induced aging treatment of rats, and significantly increase mitochondrial membrane potential. In Electro-acupuncture group, cells in G0\G1 cycle significantly increase, and ROS level significantly decrease. Conclusion: Electroacupuncture can inhibit Senescence induced by ATP injection.

Keywords: Hegu; Taichong; Electroacupuncture; ATP, Senescence.

1. Introduction

The Cellular Aging Network (SenNet) is an endeavor initiated by the National Institutes of Health (NIH) Mutual Fund aimed at comprehensively mapping senescent cells throughout their lifespan in both humans and mice. The burgeoning life expectancy observed in developed nations has precipitated a surge in age-related chronic ailments. Over recent decades, multiple studies have underscored the pivotal role of cellular aging in the etiology of many of these maladies. Senescent cells exhibit hallmark features such as cell cycle arrest, evasion of apoptosis, and the acquisition of an aging-related secretory phenotype (SASP), leading to heightened secretion of diverse bioactive molecules crucial for the pathophysiology of aging [1,2]. Cellular senescence stands as a recognized instigator of aging and age-associated ailments, representing a fundamental biological process characterized by irreversible growth arrest and alterations in cellular function implicated in a myriad of physiological and pathological contexts, including age-related diseases and the progression of cancer.

Senescence manifests in white adipose tissue (WAT) following a two-week high-fat diet (HFD), evidenced by augmented ß-galactosidase activity associated with WAT senescence and heightened expression of cyclin-dependent kinase inhibitors 1A and 2A. WAT senescence exerts its influence across various WAT cell subsets, encompassing preadipocytes, adipose tissue progenitor cells, immune cells, and adipocytes. The aging of WAT correlates with elevated glycolytic activity and mitochondrial function, leading to heightened ATP levels in HFD-induced preadipocytes compared to those derived from a standard diet. Notably, after five weeks on the HFD, a month-long regimen of daily exercise emerges as an efficacious ameliorative strategy, reversing cellular aging in WAT while concurrently diminishing glycolytic metabolism and ATP synthesis [3]. These findings underscore the pivotal role of HFD-induced ATP upregulation as a localized danger signal precipitating WAT senescence. Furthermore, adenosine triphosphate (ATP), an omnipresent molecule crucial in cellular energy metabolism, has emerged as a pivotal modulator of aging pathways. ATP-mediated signaling cascades contribute to the promotion of cellular senescence via diverse mechanisms, including oxidative stress, DNA damage, and inflammation.

Despite considerable strides in elucidating the molecular intricacies of aging, therapeutic modalities for age-related ailments remain circumscribed. Traditional Chinese medicine, notably Electroacupuncture, has garnered escalating interest

for its prospective capacity to modulate cellular processes and assuage age-related maladies. Hegu Point (LI4) and Taizhong Point (LR3) are two Electroacupuncture locales acclaimed for their efficaciousness in traditional Chinese medicine. Nonetheless, their potential in ameliorating ATP-induced aging and the underlying mechanisms remain inadequately elucidated. Recent investigations have unveiled that Electroacupuncture stimulation can wholly or partially reverse the expression profile of specific genes during hippocampal aging. Simultaneously, genes unrelated to cerebral aging were also susceptible to Electroacupuncture's influence. In parallel, non-acupoint interventions exert certain effects on the expression of age-associated genes, albeit with marginal or adverse repercussions on their expression [4]. Electroacupuncture intervention markedly augments triosephosphate isomerase (TPI) activity in the hippocampus of rats. These findings imply that the cognitive decline observed in SAMP8 mice with advancing age might stem from diminished TPI activity. By elevating TPI activity, Electroacupuncture purportedly ameliorates cognitive dysfunction, rectifies aberrant glycolytic metabolism, and preserves cerebral homeostasis and internal milieu [5].

Hegu, also known as Tiger Mouth, is a pivotal point in Traditional Chinese Medicine, described in the Spiritual Pivot. It pertains to the Hand Yangming Large Intestine channel and serves as the original point. Situated on the dorsum of the hand, between the first and second metacarpal bones, it lies precisely at the midpoint of the second metacarpal bone. Alternatively, it can be located by placing the thumb phalangeal joint of one hand transversely across the web edge between the thumb and index finger of the other hand, with the tip of the thumb falling directly onto the point. This area is traversed by the superficial branch of the radial nerve, the deep medial nerve of the palmar proper nerve, and a dorsal vein network of the hand, with the radial artery proximally positioned from the dorsum of the hand to the palm. Hegu primarily functions to invigorate the flow of qi and blood at the Tianbu level, facilitating the transport of nourishing cloud qi to the Tianbu level.

Taichong, also known as Dachong, is another meridian point delineated in the Spiritual Pivot, belonging to the liver channel of Foot Jueyin. Positioned on the dorsum of the foot, between the first and second metatarsal bones, it resides in the anterior depression at the junction of the metatarsal bones or at the site where arterial pulsations are palpable. This area encompasses the dorsal venous network of the foot and the first dorsal metatarsal artery. Additionally, it is traversed by the dorsal nerve of the deep peroneal nerve and the lowest medial nerve of the tibial nerve. Taichong's principal functions encompass the pacification of liver yang and dispelling wind, clearing heat and promoting diuresis, as well as dredging collaterals and alleviating pain.

With the increasing incidence of age-related ailments and the constrained efficacy of existing therapeutic approaches, there exists a pressing imperative to delve into novel avenues for ameliorating aging and its associated maladies. To date, the phenomenon of senescence induced by excessive extracellular ATP and its amelioration through Electroacupuncture remain unexplored. Thus, the primary objective of this investigation is to assess the therapeutic efficacy of Hegu electroacupuncture and Taichong electroacupuncture in mitigating ATP-induced senescence while unraveling their underlying molecular mechanisms. By delineating the interplay between ATP signaling and Electroacupuncture-mediated modulation of aging pathways, this study endeavors to furnish novel insights into prospective treatment modalities for age-related diseases and the progression of cancer.

2. Methods

2.1. Modeling of Rats

In this investigation, 60 specific pathogen-free (SPF) Sprague-Dawley (SD) rats, comprising an equal number of males and females, were procured from Gansu University of Traditional Chinese Medicine. The experimental animal production license number was SCXK (Liao) 2019-0004. All animals were aged between 6 to 8 weeks and exhibited a body mass within the range of (250±20) g, housed in the SPF animal laboratory of Gansu University of Chinese Medicine. Standardized feeding protocols and environmental controls were enforced, with a one-week acclimatization period preceding the experiment. This study obtained approval from the Animal Experiment Ethics Committee of Gansu University of Chinese Medicine (Ethics No. 21000042023189), ensuring compliance with the Guiding Opinions on Treating Experimental Animals.

For Electroacupuncture procedures, Huatuo brand Electroacupuncture needles measuring 0.25mm × 13mm were utilized. The 60 rats were randomly divided into five groups: the control group received injections of normal saline, the model group received ATP solution injections, and the intervention groups underwent electroacupuncture at frequencies of 20Hz, 30Hz, and 50Hz, respectively.

ATP injections in human patients are typically administered intravenously at dosages ranging from 10 to 40mg per day for individuals weighing 60kg. To determine the equivalent dosage for rats, conversion based on body surface area is necessary, considering the approximate ratio of 6.25:1 between human and rat surface areas. Employing linear interpolation, the daily dose conversion for rats corresponds to the minimum dose (10 mg) as 10 mg × (6.25/60), and for the maximum dose (40 mg) as 40 mg × (6.25/60). The injections were administered once daily for a duration of 2 weeks, and observations were made for licking, biting, or shaking behaviors. Intervention occurred within 0-24 hours after successful modeling, with bilateral Hegu and Taichong Electroacupuncture conducted once daily for 20 minutes each session.

2.2. Gene Sequencing

Blood RNA was extracted using the TRIzol method, followed by gene sequencing. Specifically, RNA was extracted utilizing the TRIzol method, and 1 μL was utilized for quantification using a Nanodrop instrument. Based on the quantitative results, 500 ng of 1% agarose was employed for electrophoresis detection, with supplementation of the end of dscDNA post-synthesis. Subsequently, 12.5 μL of A-tailing buffer was added to 17.5 μL of DNA, thoroughly mixed, and incubated at 37℃ for 30 minutes. Following this, PCR enrichment was performed after spligation, and the RNA library was quantified using Qubit. Illumina Hiseq 3000 sequencing was carried out subsequent to cluster formation using the Start cBot instrument.

2.3. Differential Gene and Intersection Gene

The DESeq2 software was employed to analyze the gene sequencing data from the aforementioned two groups.

Differential genes meeting the criteria of |log2FC|≥1 and $P \leq 0.05$ were identified between the groups. Additionally, "senescence" gene data were retrieved from the NCBI gene database and overlapped with the sequencing data.

2.4. Enrichment Analysis and Module Analysis

Biological and functional annotation of target genes was conducted using R language and the Bioconductor package. Gene set enrichment analysis (version 3.0) was employed for GO analysis and KEGG enrichment analysis to determine statistically defined gene sets (http://software. broadinstitute. org/gsea/). A screening condition of $P < 0.05$ was applied, with smaller P values indicating greater abundance, which is indicative of important biological processes and pathways. Gene set variation analysis (GSVA) was utilized as a nonparametric, unsupervised method to assess transcriptomic gene enrichment. By scoring the gene set of interest comprehensively, GSVA converts gene-level changes into pathway-level changes, thereby elucidating the biological function of the sample. Gene sets were downloaded from the Molecular Signatures Database (version 7.0), and each gene set was comprehensively scored using the GSVA algorithm to evaluate potential biological functional changes in different samples. The protein-protein interaction (PPI) network diagram was exported from STRING, and hub genes of the gene sequencing results were screened based on the central degree of nodes.

2.5. Analysis of miRNA-mRNA Regulatory Network

Bioinformatics tools and databases, such as TargetScan, were employed to predict the miRNAs targeted by differentially expressed mRNA. Regulatory networks were constructed using Cytoscape.

2.6. RT-qPCR Detection

The ice bath was prepared to thaw the reagents on ice for subsequent use. Blood in each group were cultured until 90% of the bottom of the culture bottle was covered. The collected Blood were then transferred into 1.5ml enzyme-free EP tubes, and 1ml pre-cooled Trizol was added to each tube. Ultrasound was utilized to disrupt the samples, followed by a 30-minute incubation at 4℃ to fully dissociate the ribosomes. 1/5 volume of chloroform was introduced to the lysate, vigorously shaken for 15 seconds, and allowed to rest on ice for 5 minutes. The mixture was centrifuged at 4℃, 12000r/min for 15 minutes, and the upper aqueous phase was carefully transferred to a fresh centrifugal tube. Then, before centrifuging at 12000 rpm for 10 minutes at 4°C, 1/2 volume of isopropyl alcohol was added, completely mixed by inversion, and left to stand at room temperature for 10 minutes. The supernatant was discarded, and the pellet was washed with 1mL 75% ethanol, followed by centrifugation at 4°C, 12000r/min for 10 minutes. The pellet was allowed to air dry for ten minutes at room temperature after repeating the ethanol wash phase. The RNA pellet was dissolved in 20μL of RNase-free water, and the concentration and purity of RNA were evaluated using a Q5000 ultraviolet spectrophotometer. It was ensured that the A260nm/A280nm ratio fell within the range of 1.8-2.0 for subsequent experiments, and any residual RNA was stored at -80℃ for future use.

According to the system formula, the reaction mixture was added into the sterilization PCR tube of RNAse free on ice: 1) 12μL RNase free ddH2O; 2) 3μL 5×gDNA digester, rapid centrifugation, incubation at 42℃ for 2 min, total 15μL. After finishing, the PCR reaction tubes of each group were placed on ice, the following reagents were added (Table 1), and the tubes were rapidly centrifuged to observe that there were no droplets on the wall of the tubes and no bubbles at the bottom of the tubes. The reaction conditions were as follows: 25℃ for 5 min, 5℃ for 15 min, 85℃ for 5 min on the PCR reaction meter. The synthesized cDNA was stored in the refrigerator at -80℃ for subsequent experiments.

Table 1. Reverse transcription reaction system (prepared on ice)

Constituent	Usage amount
cDNA	15μl
4×Hifair® III Supermix plus	5μl

Primer design: The sequence of gene primers is shown in Table 2.

Table 2. qRT-PCR primer sequence

Gene (Rabbit)	Prime	Product length
GAPDH	F:GCAAAGTGGATGTTGTCGCC R:TGATGACCAGCTTCCCGTTC	132
HSPA4	F: ACCACCTCAAGCAAAGAAGG R:CCGTTCCTTCTCCAGTTTATCC	154
CASP3	F:ATGGAGAACAACAAAACCTCAGT R: TTGCTCCCATGTATGGTCTTTAC	115
AKT1	F: ATGGACTTCCGGTCAGGTTCA R: GCCCTTGCCCAGTAGCTTCA	195
PARP1	F: ACCACGCACA ATGCCTATGA R: AGTCTCCGGTTGTGAAG CTG	102
NFKB1	F: CTGAGTCCCGCCCCTTCTAA R: CCTCTGTGTAGCCCATCTGTC	200
GSK3B	F: AGA CCAATAACGCCGCTTCT R:TGACCAGTGTTGCTGAGTGG	120
FOXO3	F: CCAGTGACTTGGACCTGGAC R:TCCCCACGTTCAAACCAACA	173

Quantitative PCR reaction system was configured, as shown in Table 3. The primer was designed and synthesized by Gansu Ke BiotechnologyCo., LTD. The primer sequences online server (https://www.ncbi.nlm.nih.gov/tools/primer-blast/).

Table 3. PCR reaction system

Constituent	Volume(μl)	Final concentration
Hieff qPCR SYBR Green Master Mix (low Rox)	10	1
Forward Primer (10uM)	0.4	0.2μl
Reverse Primer (10uM)	0.4	0.2μl
Template DNA	1	
Sterile ultra-pure water	8.2	

After completing the preceding experimental steps, the PCR reaction procedure was initiated. The reaction conditions were set as follows: initial denaturation at 95℃ for 5 minutes for one cycle; followed by denaturation at 95℃ for 10 seconds, annealing at 60℃ for 20 seconds, and extension at 72℃ for 20 seconds for 40 cycles. Finally, a melt curve analysis was conducted with the default settings for one cycle. Subsequently, CT values were obtained for each group, and *GAPDH* was employed as the internal reference to calculate the relative gene expression.

2.7. Apoptosis Detection

The Hoechst 33342/PI method was employed to assess apoptosis. Hoechst 33342 utilizes a krypton laser to excite ultraviolet light, with an excitation wavelength of 352 nm and an emission wavelength ranging from 400 to 500 nm, resulting in blue fluorescence. Conversely, PI utilizes an argon ion laser to excite fluorescence, with an excitation light wavelength of 488 nm and an emission light wavelength greater than 630 nm, producing red fluorescence. The cells were suspended in 1 mL of cell staining buffer, combined with 5 uL of Hoechst staining solution and 5 uL of PI staining solution, and then incubated at 4°C for 20-30 minutes. Subsequently, the apoptosis rate was assessed via flow cytometry.

2.8. Cell Cycle Detection

Staining methods employing Propidium Iodide (PI) were utilized to investigate alterations in the cell cycle. Preparation of the PI staining solution involved adding 25μl of Propidium Iodide stain solution (20x) and 10μl of RNaseA (50x) to 0.5mL of stain buffer for flow detection. Red fluorescence emitted at an excitation wavelength of 488nm was detected, while light scattering was assessed via flow cytometry. Cell DNA content and light scattering data were subsequently analyzed using suitable analysis software.

2.9. Flow Cytometry was used to Detect ROS Levels

DCFH-DA was diluted with serum-free medium at a ratio of 1:1000 to achieve a final concentration of 10μmmol/L. The DCFH-DA was then washed with PBS three times to thoroughly eliminate any DCFH-DA that had not entered the cell. Typically, the positive control for reactive oxygen species (ROS) involves a significant increase in ROS levels after cells are stimulated for 20-30 minutes. Only Rosup was added to the positive control well for this purpose, and detection was performed using flow cytometry with an excitation wavelength of 488nm and an emission wavelength of 525nm. Flowjo software was employed to analyze the results obtained from flow cytometry.

2.10. Detection of Mitochondrial Membrane Potential

Preparation of JC-1 staining working solution: For each well of the six-well plate, 1mL of JC-1 staining working solution is required. JC-1 was diluted by adding 8μL of ultra-pure water for every 50μL of JC-1 (200×). After vigorous shaking to fully dissolve and mix JC-1, 2mL of JC-1 staining buffer (5×) was added and thoroughly mixed to create the JC-1 staining working solution. Rh123 (working concentration: 10μg·L-1) was added to the peripheral blood precipitation at a volume of 1mL, followed by incubation at 37°C for 30 minutes in the dark. The cells were then washed twice, the supernatant was discarded, and they were subsequently washed once with 1L of PBS buffer to completely remove any residual dye. Finally, the samples were analyzed using flow cytometry.

3. Results

3.1. Identification of DGE

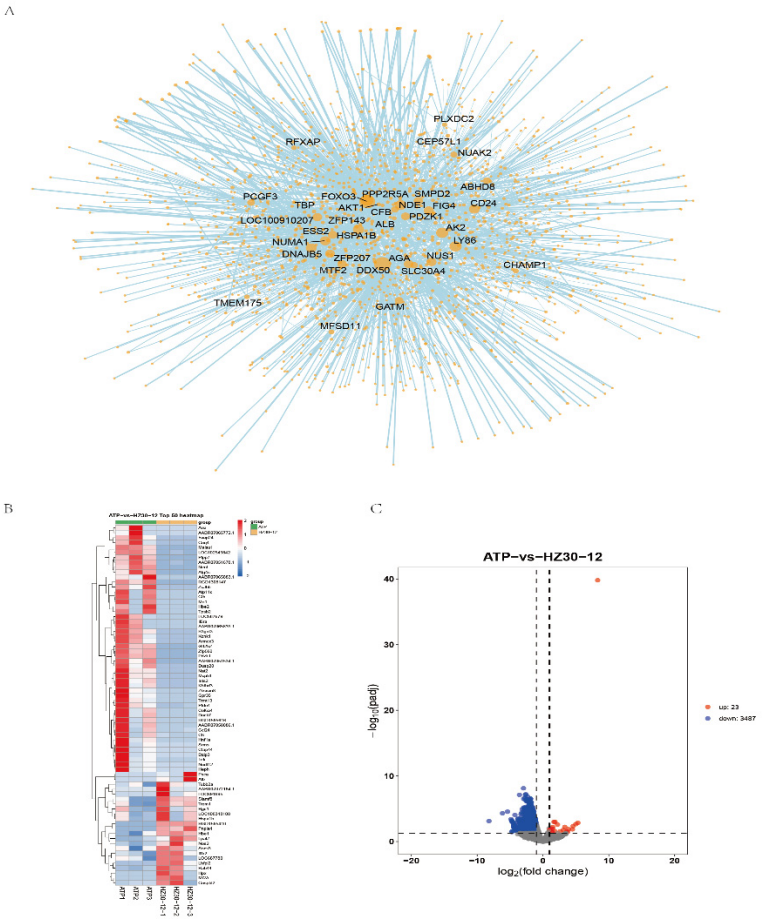

Figure 1. Analysis of genetic differences and construction of PPI: (A) Visualization of the protein-protein interaction (PPI) network was constituted by STRING. (B-C) Boxplot and heatmap of differential analysis; blue represents the control group samples, red represents the experimental group samples, '***' represents P<0.001, '**' represents P<0.01, '*' represents P<0.05

The differential gene expression (DGE) analysis unveiled 3,510 genes with significant expression variances in the sequencing dataset, comprising 3,487 genes showing upregulation and 23 displaying downregulation (Figure 1B-C). From the NCBI database, a compilation of 2,597 genes associated with aging was procured, and a Venn diagram analysis pinpointed 175 common genes among the differentially expressed genes (DEGs) and aging-related genes (Figure 2C).

3.2. Functional Enrichment Analysis

Functional enrichment analysis of the sequencing data using the Kyoto Encyclopedia of Genes and Genomes (KEGG) revealed that the identified genes primarily participate in critical pathways such as the T cell receptor signaling pathway, Human T-cell leukemia virus 1 infection, Protein processing in endoplasmic reticulum, and Phosphatidylinositol signaling system, among others (Figure 2A). Moreover, Gene Ontology (GO) analysis delineated their involvement in various biological processes (BP), including mRNA processing, mRNA splicing via spliceosome, RNA splicing via transesterification reactions, and others. In terms of cellular components (CC), enrichment was observed in nuclear speck, spliceosomal complex, and catalytic step 2 spliceosome. Molecular functions (MF) were mainly associated with transcription coregulator activity, catalytic activity acting on RNA, and catalytic activity acting on DNA (Figure 2B).

Further examination via Venn Diagram analysis identified 59 genes shared among the datasets. GO analysis of these genes highlighted enrichment in responses to ketone, cellular responses to abiotic stimulus, and positive regulation of cellular catabolic processes. Additionally, KEGG analysis indicated their involvement in pathways such as the AGE-RAGE signaling pathway in diabetic complications, Non-alcoholic fatty liver disease, and the FoxO signaling pathway, among others (Figure 2E-F).

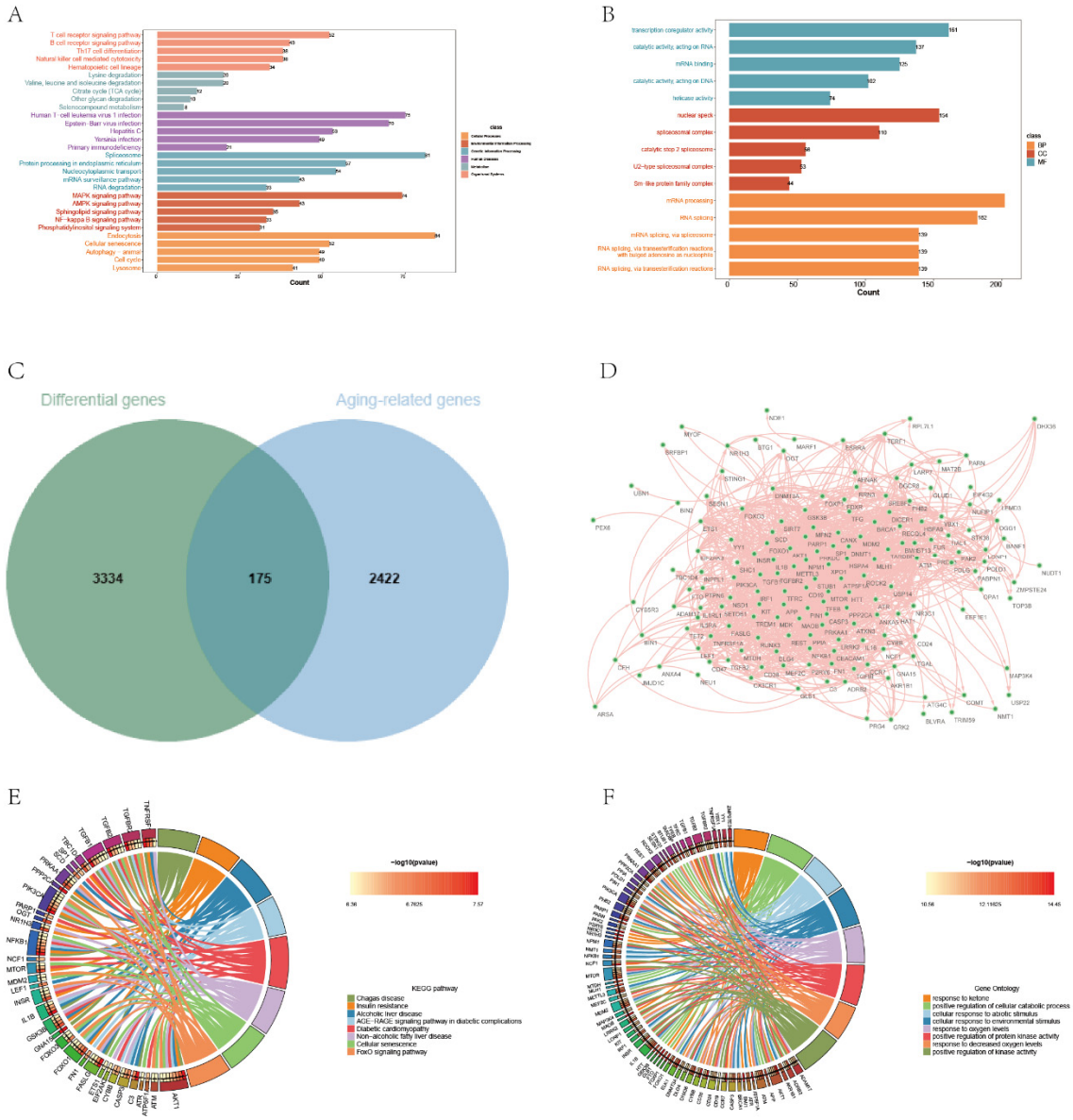

Figure 2. Enrichment analysis and screening of Aging-related genes genes: (A) KEGG enrichment analysis of differential genes. (B) GO enrichment analysis of differential genes. (C) Venn diagrams showing differential genes and Aging-related genes. (D) Construction of a PPI network map of senescence-related differential genes. (E) KEGG enrichment analysis of Aging-related differential genes. (F) GO enrichment analysis of Aging-related differential genes

3.3. PPI Network Construction and Modularization Analysis

The protein-protein interaction (PPI) network was established using the STRING database, illustrating the interconnected relationships among the proteins encoded by the differentially expressed genes obtained from the sequencing data (Figure 1A). Furthermore, the construction of the PPI network map based on age-related genes identified via Venn diagram analysis is depicted in Figure 2D. Employing Cytoscape's MCODE plug-in facilitated the identification of four core modules, encompassing a collective total of 62 shared differentially expressed genes (DEGs) (Figure 3A-D).

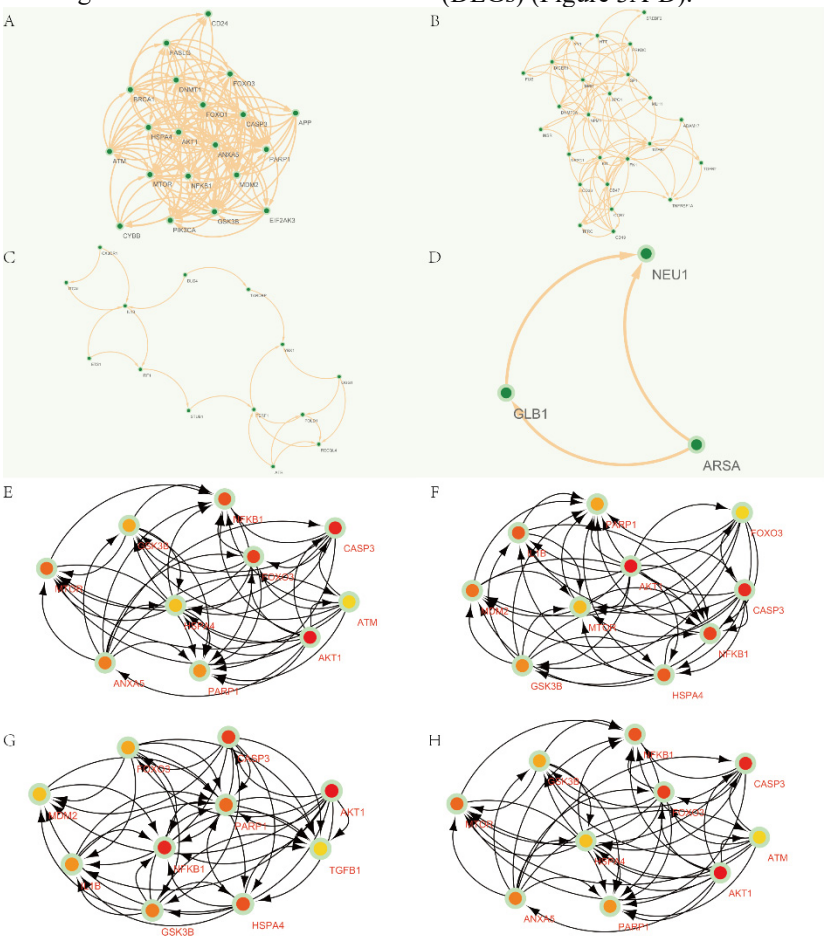

Figure 3. Shared hub genes identification and functional interaction network diagram. (A-D) The top 10 core genes identified by Degree,MNC,EPC and MCC algorithms using the Cytohubba plugin in Cytoscape. (E-H) key gene modules identified by the MCODE plug-in in Cytoscape

3.4. Selection and Analysis of Hub Genes

Utilizing the CytoHubba plug-in within Cytoscape software, topological analysis algorithms such as Degree, EPC, MCC, and MNC were employed to ascertain the top 10 key genes within the protein-protein interaction (PPI) network (Figure 3E-H). The Venn diagram illustrates the intersection of seven core genes identified by all four algorithms: *HSPA4*, *CASP3*, *AKT1*, *PARP1*, *NFKB1*, *GSK3B*, and *FOXO3* (Figure 4A). Subsequently, seven central genes were delineated through the integration of CytoHubba and MCODE visualization plug-ins (Figure 4B). These discerned key genes are presumed to exert pivotal roles in the pathological cascade of ATP-induced aging. Leveraging the GeneMANIA database facilitated the analysis of gene co-expression networks and their associated functions. The breakdown revealed that Physical Interactions constituted 46.62%, Co-expression 22.99%, Co-localization 11.37%, Predicted 10.96%, and Pathway 8.07% (Figure 4E). KEGG analysis underscored involvement in pathways such as Alcoholic liver disease, Neurotrophin signaling pathway, and non-alcoholic fatty liver disease (Figure 4C). Moreover, GO enrichment highlighted processes like positive regulation of neuron death, regulation of polysaccharide biosynthetic process, and regulation of metabolic process, among others (Figure 4D).

3.5. Effect of Electroacupuncture on Apoptosis Level in ATP-induced Aging Therapy in Rats

To explore the impact of Electroacupuncture on apoptosis during ATP-induced senescence treatment in rats, flow cytometry was employed to assess apoptosis levels. As depicted in Figure 6, cells in the Electro-acupuncture group exhibited a notable decrease in apoptosis compared to those in the ATP group (P<0.001). These findings indicate that Electroacupuncture possesses the capability to mitigate apoptosis levels in rats undergoing ATP-induced aging therapy (Figure 5A-C, M).

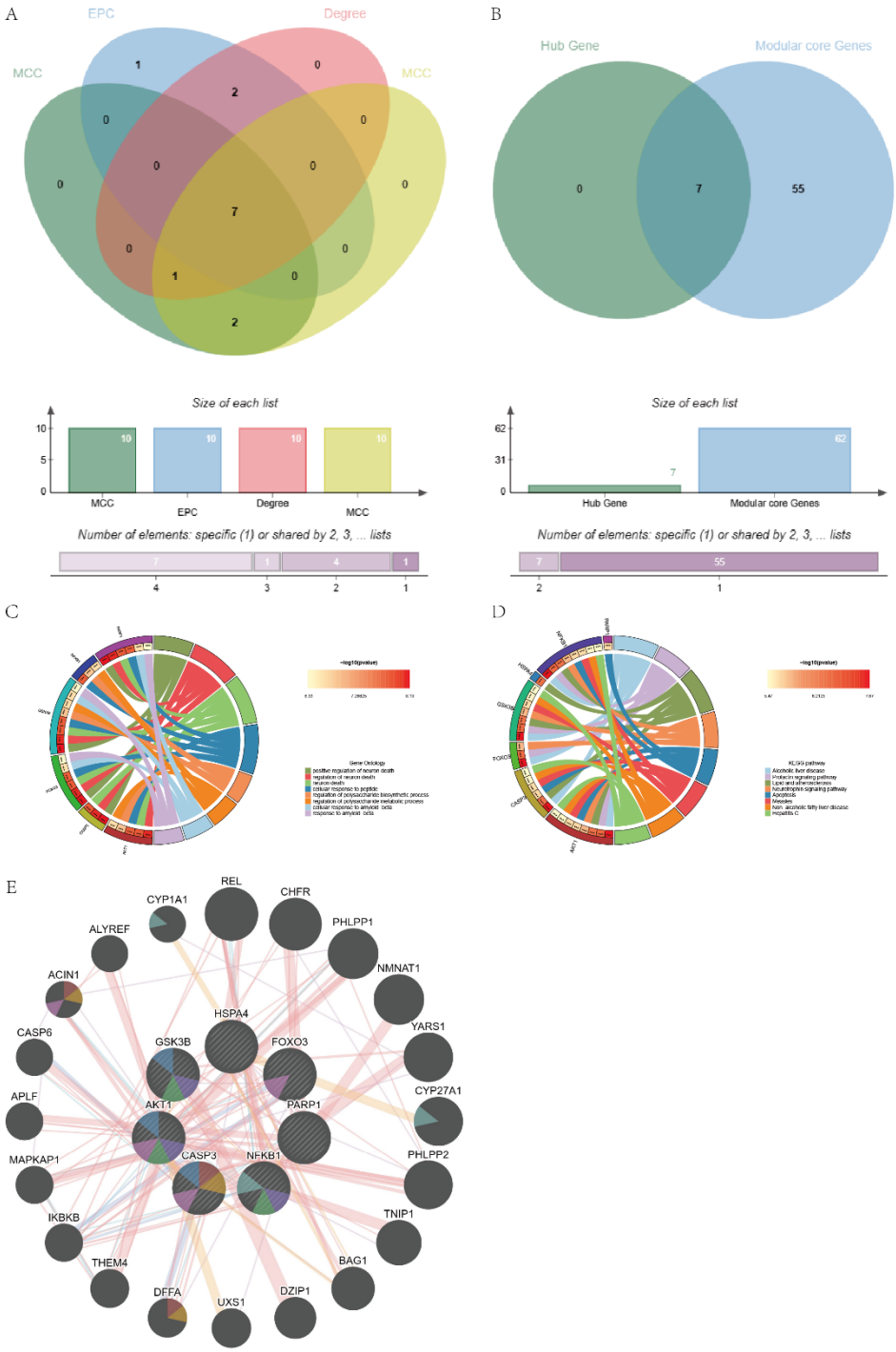

Figure 4. Shared hub genes identification and functional interaction network diagram. (A) Shared core gene venn maps were identified by the Degree, MNC, EPC and MCC algorithms using the Cytohubba plugin in Cytoscape. (B) Venn diagram showing the 7 crossover hub genes between the candidate genes of CytoHubba and MCODE. (C) GO enrichment analysis of shared genes. (D) KEGG enrichment analysis of shared genes. (E) GeneMANIA diagram illustrates the co-expression interactions between the 7 identified shared hub genes and their neighboring genes. Color codes indicate the functions shared by genes

levels in ATP-induced Aging treatment in rats. (A-C,M) Electroacupuncture on the level of apoptosis in ATP-induced Aging treatment in rats. (D-F,N) Electroacupuncture on the level of cellular mitochondrial membrane potential in ATP-induced Aging treatment in rats. (G-I,O) Electroacupuncture for cell cycle changes in ATP-induced Aging treatment in rats. (J-L,P) Electroacupuncture for cellular ROS levels in ATP-induced Aging treatment in rats.

3.6. Effects of Electroacupuncture and Moxibustion on Mitochondrial Membrane Potential Levels in ATP-induced Aging Therapy in Rats

The findings revealed a significant increase in mitochondrial membrane potential in the Electro-acupuncture group compared to the ATP group (P<0.001). This suggests that Electroacupuncture intervention can enhance cellular mitochondrial membrane potential levels during ATP-induced aging therapy in rats (Figure 5D-F,N).

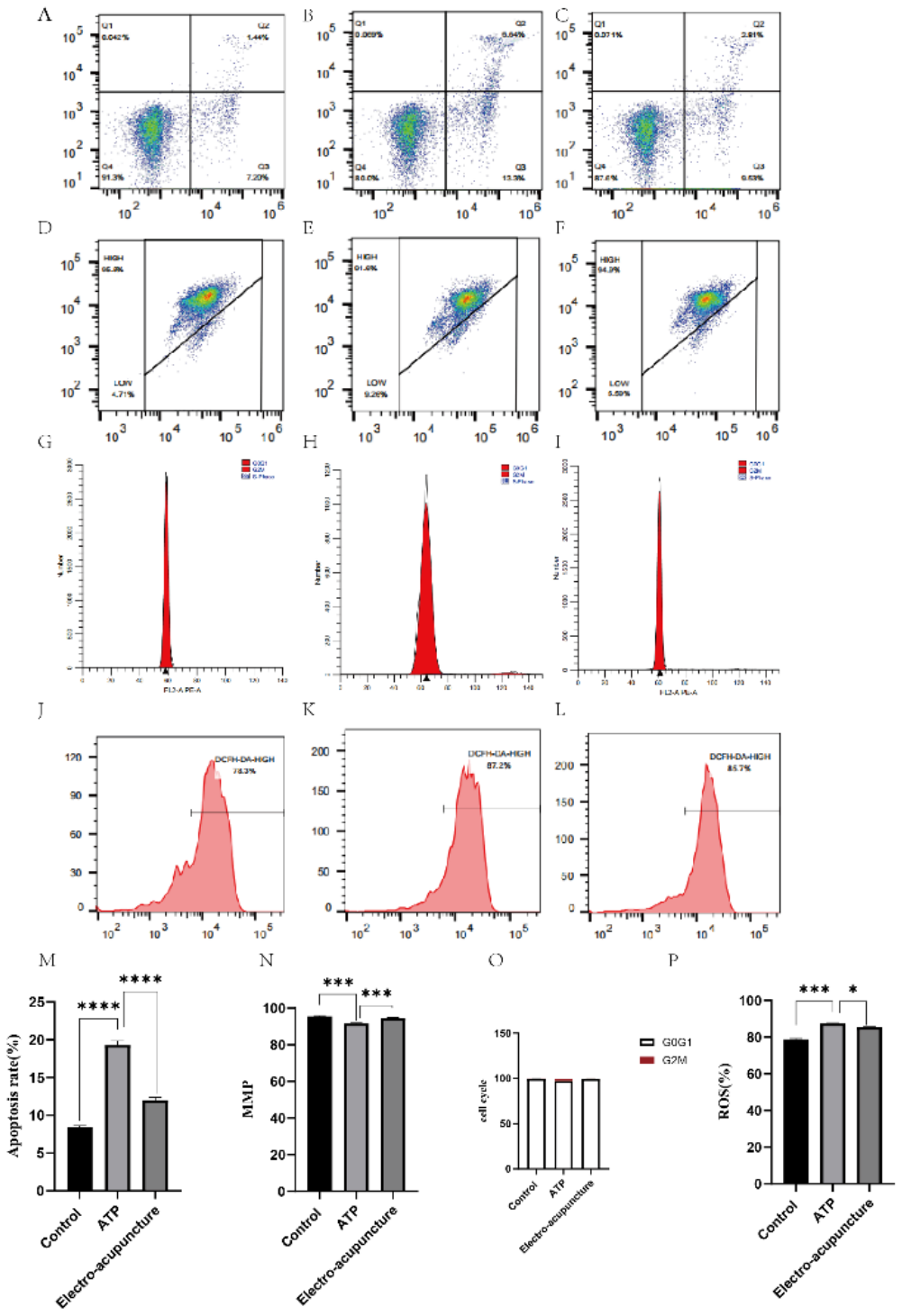

Figure 5. Effects of Electroacupuncture on apoptosis, mitochondrial membrane potential, cell cycle, and ROS

3.7. Effect of Electroacupuncture on Cell Cycle in ATP-induced Senescence Treatment in Rats

Cell proliferation can be divided into three stages: 1. The early stage of DNA synthesis, that is, the G1 stage; 2. DNA synthesis phase, that is, S phase; 3. The mitotic phase, or G2 phase. Cells in different periods have different sensitivity to drugs, and different drugs can be selected to improve the therapeutic effect according to their sensitivity differences. In this experiment, the cell cycle of each group was detected by flow cytometry according to the instructions in the cycle kit. The results showed that, compared with ATP group, the cells in Electro-acupuncture group in G0\G1 cycle significantly increased (P<0.05) (Figure 5G-I,O).

3.8. Effects of Electroacupuncture and Moxibustion on Cellular ROS Levels in ATP-induced Aging Therapy in Rats

The fluorescence probe method was employed to assess the impact of Electroacupuncture on cellular ROS levels in ATP-induced aging therapy in rats. The findings indicated a significant reduction in ROS levels in the Electro-acupuncture group compared to the ATP group (P<0.001) (Figure 5J-L,P).

3.9. RT-qPCR Detection

In comparison to the control group, the expression level of *PARP1* in cells treated solely with ATP exhibited a significant decrease (P<0.05). Conversely, the expression levels of *HSPA4*, CASP3, *AKT1*, *NFKB1*, *GSK3B*, and *FOXO3* were significantly elevated (P<0.05). Conversely, compared to the ATP group, the Electro-acupuncture group demonstrated a notable decrease in the expression levels of *HSPA4*, *CASP3*, *AKT1*, *NFKB1*, *GSK3B*, and *FOXO3* (P<0.05). Interestingly, the expression level of *PARP1* was significantly increased (P<0.05). These findings suggest that Electroacupuncture has the potential to suppress the expression levels of *HSPA4*, *CASP3*, *AKT1*, *NFKB1*, *GSK3B*, and *FOXO3* in ATP-induced aging rats while enhancing the expression level of *PARP1* (Figure 6).

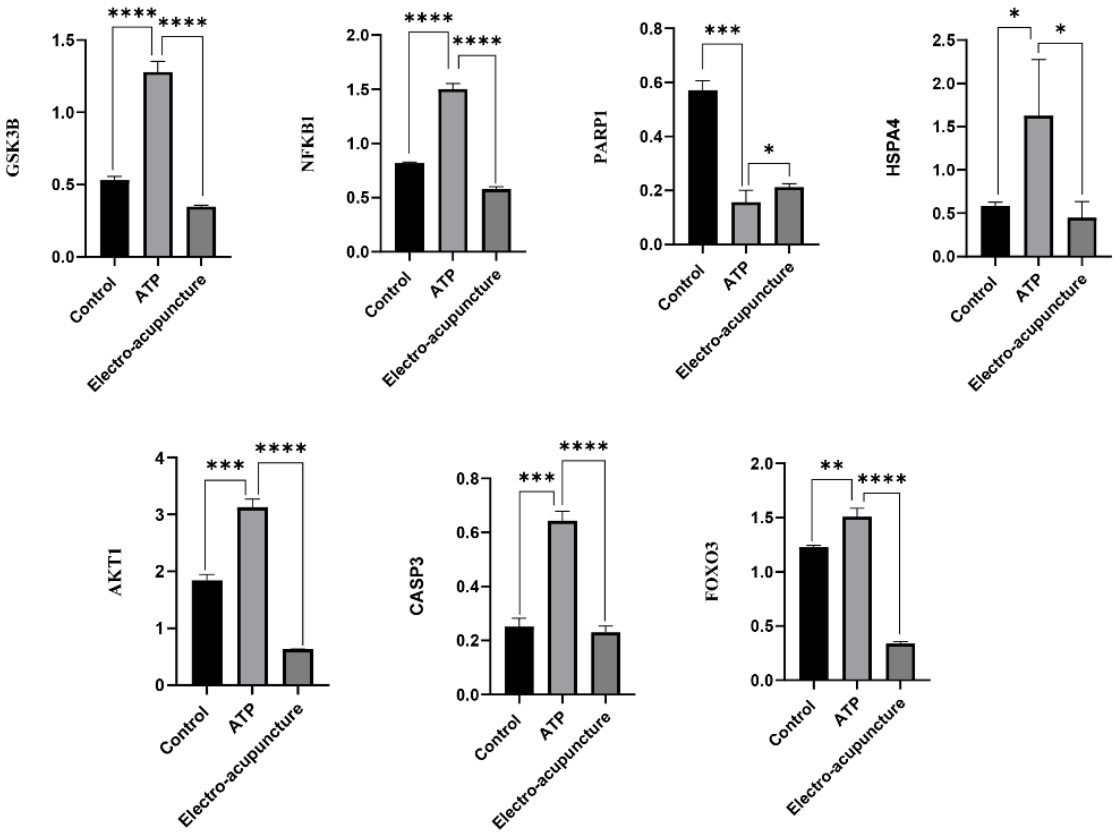

Figure 6. Shows the effect of Electroacupuncture on mRNA expression levels of HSPA4, CASP3, AKT1, PARP1, NFKB1, GSK3B and FOXO3 expression levels in the blood of ATP-induced Aging treated rats

4. Discussion

Aging is conventionally perceived as an inherent process of programmed decline culminating in mortality. This developmental trajectory is observed across diverse tissues, each with distinct physiological objectives [6]. However, contemporary research has redefined cellular senescence not merely as an endpoint of aging but as a pivotal driver of tissue remodeling during embryonic development and tissue injury. To accomplish this, senescent cells halt their proliferation, attract phagocytic immune cells, and facilitate tissue regeneration. In contexts of aging or pathological conditions, the sequential events of aging, subsequent clearance, and subsequent regeneration may be compromised, leading to the accumulation of senescent cells. Mounting evidence suggests the dual benefits of both pro-aging and anti-aging interventions. Pro-aging therapies, in scenarios such as cancer and active tissue repair, mitigate damage by restraining proliferation and fibrosis, respectively. Conversely, anti-aging interventions hold promise in eliminating accumulated senescent cells and reinstating tissue functionality [7].

In the context of electroacupuncture intervention against ATP-induced aging, the Kyoto Encyclopedia of Genes and Genomes (KEGG) analysis revealed significant involvement of pathways such as the AGE-RAGE signaling pathway in diabetic complications, non-alcoholic fatty liver disease, and the FoxO signaling pathway, among others. Despite the recognized role of advanced glycation end products (AGEs) derived from both exogenous sources like food and endogenous non-enzymatic glycation in age-related signaling pathways and aging-associated diseases, their precise contribution to aging remains elusive. Notably, the upregulation of the AGE receptor (RAGE) during aging is pivotal for the pro-lipogenic function in pre-aging adipocytes, where it mediates impaired p53 expression and function, thus impacting p21 expression [8]. The interaction between RAGE and its ligands predominantly triggers a pro-inflammatory response, often precipitating events conducive to mitochondrial dysfunction or cellular aging. Hence, RAGE assumes the role of a pattern recognition receptor (PRR), akin to those governing innate immunity, which is centrally involved in age-associated inflammation. Besides the age-related buildup of pathogen-associated molecular patterns (PAMPs) and damage-associated molecular patterns (DAMPs), along with increased pro-inflammatory cytokines from senescent and damaged cells, PRRs play a crucial role in inflammation. We posit that RAGE, through its intricate connections with immunity, aging, mitochondrial dysfunction, and inflammasome activation, drives inflammation, and the anti-aging effects observed upon RAGE blockade or deletion

stem from mitigated inflammation [9]. Moreover, advanced glycosylation end product receptor (RAGE) and STAT5 exhibit elevated expression levels in aged human kidneys and artificially aged human mesangial cells exposed to AGEs. Notably, gene and drug ablation of STAT5 markedly downregulate p16 levels and the percentage of β-gal-positive senescent cells in mesangial cells and kidneys of Sprague Dawley rats, implicating STAT5 signaling in age-induced senescence. Furthermore, AGE accumulation disrupts the protective role of autophagy in aging via the RAGE/STAT5 axis. The inhibition of autophagy by 3-methyladenine exacerbates the renal aging phenotype without activating RAGE, highlighting the pivotal role of the RAGE/STAT5-induced autophagy inhibition in mesenteric aging. Thus, the AGE-RAGE signaling pathway emerges as a crucial nexus in the aging process [10].

In recent years, cellular senescence has garnered significant attention among researchers due to its implications in both the natural aging process and prevalent human ailments. During aging, cellular transformations encompass telomere shortening, nuclear expansion, and genomic as well as mitochondrial DNA impairments, culminating in irreversible cessation of the cell cycle and the release of pro-inflammatory cytokines. This intricate process of aging contributes to the onset of numerous chronic conditions, spanning metabolic dysregulation and inflammatory disorders, as well as disease pathogenesis and tumor formation. Notably, recent investigations involving both human subjects and animal models have underscored the role of aging in initiating and progressing hepatic steatosis, including its advancement to nonalcoholic steatohepatitis (NASH). The distinctive features of NASH include heightened inflammation, hepatocellular spheroidization, and liver fibrosis. Moreover, the progression of non-alcoholic fatty liver disease (NAFLD) to NASH often coincides with various pathophysiological phenomena, such as metabolic imbalance and hepatic inflammation, which may precipitate or be instigated by cellular senescence. Thus, cellular senescence emerges as a multifaceted element that serves as both an instigator and a consequence of the disease process [11].

FOXO and p53 proteins serve as transcription factors that orchestrate various signaling pathways, governing cell cycle progression, apoptosis, and metabolism. Over the past decade, both FOXO and p53 have emerged as pivotal players in the aging process [12]. The depletion of FOXO3a RNA and protein in human dermal fibroblasts (HDFs) instigates several aging-related phenotypes, encompassing alterations in cell morphology, heightened population doubling, increased staining for aging-associated β-galactosidase, elevated levels of cellular reactive oxygen species, and upregulation of p53/p21 protein expression. These findings furnish compelling evidence regarding the indispensable role of FOXO3a transcription factor as a mediator of cellular aging, thereby underscoring the conservation of the aging mechanism [13].

In comparison to the control group, the cells treated solely with ATP exhibited a notable reduction in the expression level of *PARP1*. Concurrently, there was a significant increase observed in the expression levels of *HSPA4*, *CASP3*, *AKT1*, *NFKB1*, *GSK3B*, and *FOXO3*. Conversely, when juxtaposed with the ATP group, the Electro-acupuncture group displayed a noteworthy decrease in the expression levels of *HSPA4*, *CASP3*, *AKT1*, *NFKB1*, *GSK3B*, and *FOXO3* ($P<0.05$). Notably, the expression level of *PARP1* exhibited a significant increase. These findings suggest that Electroacupuncture holds the potential to suppress the expression levels of *HSPA4*, *CASP3*, *AKT1*, *NFKB1*, *GSK3B*, and *FOXO3*, while concurrently augmenting the expression level of *PARP1* in ATP-induced aging rats.

PARP-1 and NF-κB-associated secretomes, referred to as PNAS, are evident in non-melanoma cells. Crucially, the inhibition of PARP-1 or NF-κB effectively impedes the invasiveness of the secretome [14]. SREBP1c likely assumes a pivotal role in maintaining genomic stability and regulating aging in adipocytes by orchestrating the DNA damage response. Notably, SREBP1c exhibits an unexpected association with *PARP1*, thereby augmenting *PARP1* activity during DNA repair, independently of its conventional lipogenic function. Deletion of the SREBP1c gene accelerates adipocyte aging, leading to immune cell aggregation in obese adipose tissue. These deleterious effects precipitate maladaptive adipose tissue remodeling and insulin resistance in obesity [15]. Human premature aging is characterized by highly specific pathways, including the DNA damage response (DDR) and epigenetic modifiers, alongside distinctive determinants such as aging-related secretory phenotypes and asp-mirnas. *PARP1* is intricately involved in nucleolar processes, encompassing rRNA transcription, ribosome biogenesis, maintenance of heterochromatin and nucleolar architecture, and regulation of the release of critical DDR proteins from the nucleolus to the nucleus, thereby tethering *PARP1* to cellular senescence and nucleolar function [16]. A paramount challenge lies in unraveling the intricate interplay among candidate elements and delineating their respective contributions to aging, with the ultimate objective of identifying novel avenues for devising anti-aging interventions or mitigating age-related manifestations. While acknowledging the inevitability of aging and the impossibility of eradicating it entirely, extending the duration of healthy lifespan stands as a commendable objective worthy of earnest pursuit [17].

Telomerase activation serves as a safeguard against telomere damage, effectively stalling aging processes and conferring cellular immortality, while its inhibition precipitates rapid aging or triggers apoptosis. In P16-deficient lung cancer cells or tumors, telomerase instability arises from the suppression of sphingosine kinase 2 (SPHK2) and sphingosine 1-phosphate (S1P), which bind to and stabilize telomerase, thereby instigating telomere damage-triggered caspase-3 activation and apoptosis, rather than senescence. These outcomes were averted upon knockdown of the tumor suppressor protein transcription factor 21 (TCF21) or ectopic expression of wild-type human telomerase reverse transcriptase (hTERT), but not by manipulating the S1P-binding mutant hTERT. Intriguingly, SPHK2-deficient mice exhibited accelerated aging and telomerase instability, coupled with heightened telomere damage and aging via p16 activation, particularly in testicular tissue, while evading apoptosis. Furthermore, silencing p16 in SphK2−/− mouse embryonic fibroblasts triggered caspase-3 activation and apoptosis sans senescence induction. Notably, in P16-deficient A549 lung cancer cells, ectopic expression of wild-type p16 thwarted TCF21 and caspase-3 activation, impeding SphK2/S1P inhibition and precipitating aging accompanied by telomere damage [18]. These findings underscore the direct involvement of p16 in telomere damage-dependent aging by sequestering caspase-3 to curb apoptosis, thereby revealing a direct nexus between telomere damage-dependent

aging and apoptosis in the context of aging and cancer. During replicative senescence, cells undergo permanent withdrawal from the cell cycle. Conventionally, this occurs following successive passages, marking the culmination of the culture's in vitro lifespan. Evidence suggests that replicating senescent fibroblasts resist apoptotic demise, attributed to the deficiency in key enzyme activity, with caspase-3 serving as the principal executor [19].

In human CD8+ T lymphocytes subjected to prolonged culture, the modulation of TNF-α levels through chronic exposure to neutralizing antibodies or TNF-α receptor-1 inhibitors demonstrates the potential to augment proliferation, forestall the loss of CD28 expression, defer alterations in cytokine profiles, and bolster telomerase activity. Corroborating the in vitro findings, CD8+CD28−T lymphocytes exhibited markedly elevated levels of caspase-3 compared to CD28+ counterparts in vitro assays [20].

The AKT kinase family comprises three distinct subtypes, each playing both unique and overlapping roles in cancer progression. Often exhibiting hyperactivity in various cancers, including melanoma, they have also been implicated in the modulation of aging processes. Recent investigations into the CGAS-STING pathway, crucial in cellular aging, have unveiled a dependency of CGAS-STING functionality on *AKT1*. Interestingly, pharmacological inhibition of cGAS exerts minimal influence on aging, whereas we have observed that the SASP factor necessitates NF-κB activity and is partly contingent on *AKT1*-induced phosphorylation of IKKα [21].In Akt1−/−mef cells, subjected to ultraviolet irradiation, phenotypic alterations indicative of aging are evident. These changes include cellular enlargement and flattening, decreased proliferation, and augmented staining for age-related β-galactosidase (SAβ-gal), signifying premature aging in Akt1−/−mef cells post-ultraviolet exposure. Conversely, restoration of Akt1 expression in Akt1−/−mef cells suppresses SAβ-gal activity, suggesting that UV-induced aging stems from Akt1 dysfunction. Notably, under ultraviolet irradiation, levels of reactive oxygen species (ROS) escalate rapidly, and the ROS scavenger NAC mitigates UV-induced aging in Akt1−/−MEFs, underscoring the regulatory role of UV-induced intracellular ROS levels in the premature aging of Akt1−/−MEFs [22].

The versatility of the κlight polypeptide gene enhancer nuclear factor in B cell (NF-κB) pathway activation stems from the amalgamation of five subunits forming homologous and heterodimeric NF-κB complexes. While biochemical and gene knockout studies have delineated the overlapping and distinct functions of these proteins, the mechanisms dictating environment-dependent functionality, the formation of diverse dimeric complexes, and the transcriptional control of disparate stimuli remain poorly understood [23]. NF-κB stands as a principal regulator of age-associated gene expression, with the p50/NF-κB1 subunit serving as a pivotal modulator of NF-κB signaling. Aged Nfkb1−/− animals exhibited increased kyphosis, diminished cortical bone, heightened brain GFAP staining, and reduced overall lifespan compared to Nfkb1+/+ counterparts. In vitro, primary Nfkb1−/− MEFs subjected to continuous passage displayed a greater abundance of senescent cells than homogeneous Nfkb1+/+ MEFs. Moreover, Nfkb1−/− MEFs manifested an elevated presence of phospho-H2AX foci and decreased levels of spontaneous apoptosis compared to Nfkb1+/+ counterparts, a trend mirrored in the brains of Nfkb1−/− animals relative to Nfkb1+/+ ones. Ultimately, p50 DNA binding was notably diminished in aged tissues of wild-type animals compared to their younger counterparts [24].

In the realm of aging research, glycogen synthase kinase 3 (GSK3) emerges as a relatively recent focal point, bearing the guise of a mere regulator of growth and metabolism despite its multifaceted involvement in cellular adaptation [25]. Conversely, circular RNA circ-Foxo3 has garnered attention as a prominent player in the aging narrative, boasting heightened expression levels in the hearts of aged mice and patients, correlating with widespread senescence. Intriguingly, ectopic expression of circ-Foxo3 precipitates senescence and exacerbates adriamycin-induced cardiomyopathy, while silencing endogenous circ-Foxo3 attenuates aging and mitigates cardiomyopathy. These effects are mediated through interactions with anti-aging proteins ID-1 and E2F1, alongside anti-stress proteins FAK and HIF1α, prompting their cytoplasmic relocation. The discernible impact of circ-Foxo3 positions it as a promising target for pharmaceutical interventions aimed at curbing tissue aging [26].

Apoptosis and senescence serve as intrinsic safeguards within cells, countering the surge of mitotic signals triggered by activated oncogenes. Consequently, the evasion of apoptosis or senescence becomes a prerequisite for tumorigenesis, embodying the "lifeline" of cancer cells. Paradoxically, the effectiveness of anticancer therapeutics hinges on either the activation of apoptosis or the acute induction of cellular senescence [27]. In contrast to mitotic cells, post-mitotic cells like neurons or cardiomyocytes evade the aging process by virtue of their terminal differentiation. The fate of these cells is wholly contingent upon their capacity to withstand stress. Autophagy emerges as a pivotal mechanism for homeostasis, purging damaged organelles, aberrant proteins, and surplus cytoplasmic components [28].

In various mammalian cell types, including those undergoing p53 overexpression-induced or natural aging, a decline in mitochondrial membrane potential (ΔΨM) has been observed. This reduction in ΔΨM correlates with diminished responsiveness of the permeability transition pore complex (PTPC) to pharmacological agents that modulate its opening or closing. Notably, this reduced reactivity of PTPC seems to stem, at least in part, from decreased levels of the crucial PTPC constituent, adenine nucleotide translocase [29]. Cellular senescence represents a stable form of cell cycle arrest, serving as a barrier against tumorigenesis and aiding in tissue repair during early accumulation. However, the persistent presence of senescent cells can trigger inflammation, accelerate tissue aging, and contribute to the onset of severe conditions such as obesity, diabetes, and atherosclerosis [30]. Upon co-culturing with aged astrocytes, neuronal mitochondrial function undergoes alterations. In vivo studies further reveal diminished levels of mitochondrial oxidative phosphorylation (OXPHOS) proteins, alterations in REDOX states, and heightened markers of aging in older animals compared to their younger counterparts, suggesting a parallel between the observed in vitro and in vivo effects of aging astrocytes [31]. Collectively, these findings underscore the influence of the aged cellular microenvironment on mitochondrial function and overall physiological processes.

The aging process intricately undermines bodily function across various levels, leading to a gradual waning of resilience against stress, injury, and disease. Apart from alterations in gene expression and metabolic regulation, the pace of aging is closely intertwined with heightened production of reactive oxygen species (ROS) and/or active

nitrosates (RNS). Notably, targeted escalation in ROS levels emerges as a potential linchpin in instigating and perpetuating the cellular aging trajectory [32]. Sustainable aging necessitates prolonged activation of DNA damage response (DDR) signals, sustained by the continual generation of enduring ROS, a process under the regulatory purview of p38MAPK and augmented functional mitochondria. In efforts to counteract aging, pharmacological inhibition of p38MAPK was employed. Treatment with SB203580 sufficed to partially ameliorate the senescent phenotype, impeding ROS surge, curbing mitochondrial activity, and ultimately reinstating cellular proliferation [33]. Cellular senescence denotes a stable cessation of the cell cycle, a state that can be prompted in normal cells by diverse internal and external stimuli alongside developmental cues [34]. Despite its ubiquitous relevance, the definition of cellular senescence remains somewhat nebulous, often alluding to an irreversible halt in cellular proliferation.

5. Conclusion

This study elucidated the mechanism underlying electroacupuncture intervention in ATP-induced cellular senescence, identifying seven pivotal genes: *HSPA4*, *CASP3*, *AKT1*, *PARP1*, *NFKB1*, *GSK3B*, and *FOXO3*. Electroacupuncture demonstrated an inhibitory effect on apoptosis in the ATP-induced aging therapy of rats, concomitantly leading to a substantial increase in mitochondrial membrane potential. Moreover, cells subjected to electroacupuncture exhibited a notable increase in the G0/G1 cell cycle phase, alongside a significant reduction in ROS levels.

Data Availability

The datasets generated and/or analyzed during the current study are available from the corresponding author by reasonable request.

Conflicts of Interest

The authors declare no competing interests.

Acknowledgments

WW, YT, JX, YF, HF completed the experiment and writing, DS, HL, ZJ proofread the article.

National Nature Foundation (No. 81960877); Higher Education Innovation Fund of Gansu Province (No. 2021A-076); Gansu Province Science and Technology Plan (Innovation Base and Talent Plan) Project (No. 21JR7RA561); Key Laboratory of Dunhuang Medicine and Transformation, Ministry of Education, Open Fund Project (No. DHYX20-16); Special open project of Gansu Traditional Chinese Medicine Research Center (No. zyzx-2020-zx10); Nature Foundation of Gansu Province (No. 21JR1RA267); Education Technology Innovation Project of Gansu Province (No. 2022A-067); Higher Education Innovation Fund of Gansu Province (No. 2023A-088); Natural Science Foundation of Gansu Province, No. 22JR5RA582; Key Research and development Program of Gansu Province Science and Technology Plan Project International Science and Technology Cooperation category (No. 23YFWA0005), Northwest Collaborative Innovation Center for Prevention and Control of Traditional Chinese Medicine Related Diseases of Nutrition and Environment (No. ZYXT-24-02).

References

[1] Lucas, Vasco, Cláudia Cavadas, and Célia Alexandra Aveleira. "Cellular senescence: from mechanisms to current biomarkers and senotherapies." Pharmacological Reviews 75.4 (2023): 675-713.

[2] Gurkar, Aditi U., et al. "Spatial map** of cellular senescence: emerging challenges and opportunities." Nature aging 3.7 (2023): 776-790.

[3] Pini, Maria, et al. "Adipose tissue senescence is mediated by increased ATP content after a short-term high-fat diet exposure." Aging Cell 20.8 (2021): e13421.

[4] Ding, **aorong, et al. "Acupuncture regulates the aging-related changes in gene profile expression of the hippocampus in senescence-accelerated mouse (SAMP10)." Neuroscience Letters 399.1-2 (2006): 11-16.

[5] Zhao, Lan, et al. "Aging-related changes of triose phosphate isomerase in hippocampus of senescence accelerated mouse and the intervention of acupuncture." Neuroscience letters 542 (2013): 59-64.

[6] Noodén, Larry D., Juan J. Guiamét, and Isaac John. "Senescence mechanisms." Physiologia plantarum 101.4 (1997): 746-753.

[7] Muñoz-Espín, Daniel, and Manuel Serrano. "Cellular senescence: from physiology to pathology." Nature reviews Molecular cell biology 15.7 (2014): 482-496.

[8] Chen, Chih-Yu, et al. "An advanced glycation end product (AGE)-receptor for AGEs (RAGE) axis restores adipogenic potential of senescent preadipocytes through modulation of p53 protein function." Journal of Biological Chemistry 287.53 (2012): 44498-44507.

[9] Teissier, Thibault, and Éric Boulanger. "The receptor for advanced glycation end-products (RAGE) is an important pattern recognition receptor (PRR) for inflammaging." Biogerontology 20.3 (2019): 279-301.

[10] Lin, Zhihui, et al. "RAGE is a potential biomarker implicated in immune infiltrates and cellular senescence in lung adenocarcinoma." Journal of Clinical Laboratory Analysis 36.5 (2022): e24382.

[11] Papatheodoridi, Alkistis-Maria, et al. "The role of senescence in the development of nonalcoholic fatty liver disease and progression to nonalcoholic steatohepatitis." Hepatology 71.1 (2020): 363-374.

[12] Bourgeois, Benjamin, and Tobias Madl. "Regulation of cellular senescence via the FOXO 4-p53 axis." FEBS letters 592.12 (2018): 2083-2097.

[13] Kyoung Kim, Hyun, et al. "Down-regulation of a forkhead transcription factor, FOXO3a, accelerates cellular senescence in human dermal fibroblasts." The Journals of Gerontology Series A: Biological Sciences and Medical Sciences 60.1 (2005): 4-9.

[14] Ohanna, Mickaël, et al. "Senescent cells develop a PARP-1 and nuclear factor-κB-associated secretome (PNAS)." Genes & development 25.12 (2011): 1245-1261.

[15] Lee, Gung, et al. "SREBP1c-PARP1 axis tunes anti-senescence activity of adipocytes and ameliorates metabolic imbalance in obesity." Cell metabolism 34.5 (2022): 702-718.

[16] Hekmatimoghaddam, Seyedhossein, et al. "Sirt1 and Parp1 as epigenome safeguards and microRNAs as SASP-associated signals, in cellular senescence and aging." Ageing research reviews 40 (2017): 120-141.

[17] Kołacz, Kinga, and Agnieszka Robaszkiewicz. "PARP1 at the crossroad of cellular senescence and nucleolar processes." Ageing Research Reviews (2024): 102206.

[18] Selvam, Shanmugam Panneer, et al. "Balance between senescence and apoptosis is regulated by telomere damage–induced association between p16 and caspase-3." Journal of Biological Chemistry 293.25 (2018): 9784-9800.

[19] Marcotte, Richard, Chantale Lacelle, and Eugenia Wang. "Senescent fibroblasts resist apoptosis by downregulating caspase-3." Mechanisms of ageing and development 125.10-11 (2004): 777-783.

[20] Parish, Stanley T., Jennifer E. Wu, and Rita B. Effros. "Modulation of T lymphocyte replicative senescence via TNF-α inhibition: Role of caspase-3." The Journal of Immunology 182.7 (2009): 4237-4243.

[21] Bayer, Abraham L., et al. "AKT1 is required for a complete Palbociclib-Induced Senescence phenotype in BRAF-V600E-Driven Human Melanoma." Cancers 14.3 (2022): 572.

[22] Jee, Hye **, et al. "UV light induces premature senescence in Akt1-null mouse embryonic fibroblasts by increasing intracellular levels of ROS." Biochemical and biophysical research communications 383.3 (2009): 358-362.

[23] Cartwright, Tyrell, Neil D. Perkins, and Caroline L. Wilson. "NFKB1: a suppressor of inflammation, ageing and cancer." The FEBS journal 283.10 (2016): 1812-1822.

[24] Bernal, Giovanna M., et al. "Loss of Nfkb1 leads to early onset aging." Aging (Albany NY) 6.11 (2014): 931.

[25] Souder, Dylan C., and Rozalyn M. Anderson. "An expanding GSK3 network: implications for aging research." Geroscience 41.4 (2019): 369-382.

[26] Du, William W., et al. "Foxo3 circular RNA promotes cardiac senescence by modulating multiple factors associated with stress and senescence responses." European heart journal 38.18 (2017): 1402-1412.

[27] Schmitt, Clemens A. "Senescence, apoptosis and therapy—cutting the lifelines of cancer." Nature Reviews Cancer 3.4 (2003): 286-295.

[28] Vicencio, José Miguel, et al. "Senescence, apoptosis or autophagy? When a damaged cell must decide its path–a mini-review." Gerontology 54.2 (2008): 92-99.

[29] Sugrue, Mary M., and William G. Tatton. "Mitochondrial membrane potential in aging cells." Neurosignals 10.3-4 (2001): 176-188.

[30] Jana, Batakrishna, et al. "Mitochondrial membrane disrupting molecules for selective killing of senescent cells." ChemBioChem 22.24 (2021): 3391-3397.

[31] Morales-Rosales, Sandra Lizbeth, et al. "Senescence in primary rat astrocytes induces loss of the mitochondrial membrane potential and alters mitochondrial dynamics in cortical neurons." Frontiers in aging neuroscience 13 (2021): 766306.

[32] Davalli, Pierpaola, et al. "ROS, cell senescence, and novel molecular mechanisms in aging and age-related diseases." Oxidative medicine and cellular longevity 2016 (2016).

[33] Luo, Yi, et al. "Autophagy regulates ROS-induced cellular senescence via p21 in a p38 MAPKα dependent manner." Experimental gerontology 46.11 (2011): 860-867.

[34] Kumari, Ruchi, and Parmjit Jat. "Mechanisms of cellular senescence: cell cycle arrest and senescence associated secretory phenotype." Frontiers in cell and developmental biology 9 (2021): 485.